Int J Adv Manuf Technol (2016) 87:2721–2729
DOI 10.1007/s00170-016-8642-0

ORIGINAL ARTICLE

Precipitation behavior of γ' precipitates in the fusion zone of TIG welded ATI 718Plus®

G. Asala [1] · **J. Andersson** [2] · **O. A. Ojo** [1]

Received: 2 February 2016 / Accepted: 20 March 2016 / Published online: 2 April 2016

Abstract The precipitation behavior of the main strengthening phase, γ' precipitates, in ATI 718Plus® superalloy after Tungsten Inert Gas (TIG) welding and postweld heat treatments has been studied. In contrast to electron beam welding, where no γ' precipitates are reported to form in the as-welded condition, analytical transmission electron microscopy study in this work revealed the formation of γ' precipitates after the TIG welding, albeit in a non-uniform distribution manner. This is attributable to a more extensive elemental microsegregation that occurred into the interdendritic liquid and slower cooling rate during the TIG welding, which also induced the formation of interdendritic Nb-rich Laves phase particles and MC-type carbides. Theoretical calculations were performed to study the influence of Nb microsegregation, on both the kinetics and extent of γ' precipitation, and the results agree with experimental observations. It is found that the precipitation kinetics, and not the extent of γ' precipitate formation in the fusion zone, during postweld heat treatments is affected by the micro-segregation of Nb that produced Laves phase particles during the weld solidification.

Keywords Superalloy · Welding · ATI 718+

1 Introduction

ATI 718Plus® is a γ' ($L1_2$) phase strengthened nickel-based superalloy developed by ATI with an improved high-temperature performance compared to the traditional Alloy 718 superalloy that has been used for more than 50 years [1–5]. The improved elevated temperature performance is achieved by a careful compositional modification of primarily Al and Ti that results in the replacement of γ'' precipitates with a more structurally stable γ' precipitates as the key strengthening phase in the ATI 718Plus® superalloy. This has resulted in a desirable increase in the operating temperature to about 700 °C, while still maintaining the workability of Alloy 718. Also, the weldability of 718Plus® has been reported [6–8] to be fairly good compared with other γ' precipitation strengthened nickel-based alloy such as Waspaloy.

The microstructure of ATI 718Plus® superalloy welded by electron beam welding (EBW) technique has been investigated [6–8]. It is reported that elemental microsegregation occurs during the solidification of the weld, which causes solutes such as Nb, Ti, and Mo to segregate to the interdendritic regions, while Fe, W, Co and Cr segregate into the dendrite core regions. The segregation results in the formation of Laves phase particles and MC carbides in the interdendritic regions. Transmission electron microscopy of the weld region showed that no γ' precipitates were formed in the fusion zone after the EBW. In order to strengthen the weld region and to relief residual stresses, there is a need to subject the welded material to postweld heat treatment (PWHT) to form γ' precipitates in the required size and volume fraction. However, it was suggested [6] that the segregation of Nb into the interdendritic liquid and subsequent formation of Laves particle, during weld solidification, can deplete the ATI 718Plus® superalloy of adequate solutes to form the strengthening γ' precipitates in the required volume fraction during the PWHT. A similar scenario is reported for Alloy 718, where the consumption of Nb for the formation of weld interdendritic Laves phase particles and MC carbides deprives the alloy of enough Nb to form γ'' precipitates, a different strengthening phase, in the

---

✉ O. A. Ojo
Olanrewaju.ojo@umanitoba.ca

[1] University of Manitoba, Winnipeg R3T 5V6, Canada

[2] University West, Trollhattan, Sweden

necessary amount to adequately strengthen the material [9]. Most of the investigations carried out on the weld fusion zone of the ATI 718Plus® superalloy are on welds produced by EBW, as compared to the more conventional TIG welding. The objective of this present work was therefore to study the precipitation behavior of γ' precipitates in the ATI 718Plus® superalloy after TIG welding and PWHT. The precipitation reaction kinetics of γ' precipitates, during PWHT, and how it is affected by microsegregation of Nb are reported and discussed in this article.

2 Experimental procedure

The chemical composition of the ATI 718Plus® superalloy used in this study is shown on Table 1. The starting alloy was obtained in the form of 12.6 mm × 110 mm × 127 mm hot-rolled plates. Rectangular plates of 3 mm × 12.6 mm × 110 mm were machined from the as-received material using the electrical discharge machine (EDM). The oxidized surface layers on the plates were removed by surface grinding all the faces of the plates. Bead-on-plate autogenous welds were made on the prepared as-received plates by the use of a TIG welding system integrated with a 6 DOF PANASONIC VR-004 robot. The welding current and speed were maintained at 100 A DC and 200 mm/min, respectively. Welded samples with dimensions 3 mm × 3 mm × 12.6 mm were sectioned transversely to the welding direction. The specimens were divided into groups and were subjected to different solution heat treatments at 950, 982, 1050, 1000, 1150, and 1200 °C for 1 h, then cooled at different cooling rates, 500 °C/s, 25 °C, and 0.25 °C/s. After cooling from the solution treatment temperature, some of the samples were subjected to recommended [2] aging treatment (788 °C for 2 h, cooling at 55 °C/h to 650 °C, and holding at 650 °C for 8 h), and the others were isothermally aged at 788 °C for different holding times ranging from 1 min to 20 h. The samples were mounted and polished using the standard metallographic techniques. Metallographic specimens were electro-etched using either 10 % oxalic acid at 5 V for 3 s or 170 ml H_3PO_4 + 10 ml H_2SO_4 + 15 g CrO_3 at 5 V for 10 s. The fusion zone microstructure was examined and analyzed by the use of an optical microscope, a JEOL 5900 Scanning Electron Microscope equipped with an ultrathin window Oxford Energy Dispersive Spectrometer (EDS), a high-resolution Field Emission Gun (FEG) FEI Nova NanoSEM 450, and JEOL 2010F Transmission Electron Microscope equipped with EDAX ultrathin window detector. Thin foils for transmission electron microscopy (TEM) study were grinded and polished to about 100 μm and punched out in 3-mm coupons before subjecting them to dimpling and electropolishing. The electropolishing was done by the use of a twin-jet polisher in a solution of 10 % Perchloric acid and 90 % methyl alcohol at a temperature of around −40 and a voltage of 1.5 V and 1.5 A DC current. Vickers's microhardness was done by using a Buehler microhardness tester under a load of 500 N.

Table 1 Composition of ATI 718Plus® and the partition coefficient *k* determined in this study by SEMEDS analysis

Sample	Elements (Wt. %)								
	Al	Ti	Cr	Fe	Co	Nb	Mo	W	Ni
Base Metal	‘1.5	0.7	17.9	9.3	9.0	5.5	2.7	1.1	Bal
k, ATI 718Plus®	1.1	0.7	1.1	1.1	1	0.5	0.9	1.5	1

3 Results and discussions

3.1 As-welded microstructure

An optical micrograph of the weld fusion zone (transverse section) is shown in Fig. 1. The as-weld fusion zone generally exhibits a dendritic microstructure. The dendrites are fine and equiaxed in the weld interior and become coarse and columnar at regions near the fusion boundary. Scanning electron microscopy study revealed irregular-shaped secondary phase particles distributed in a semicontinuous fashion along the interdendritic regions (Fig. 2). Preliminary SEM X-ray energy dispersive spectroscopy analysis of the interdendritic irregular-shaped particles suggests that the particles are based on Laves phase and MC-type carbide. In addition, a high-resolution microscopy study with the use of a FEG-SEM revealed what appears to be 3–5-nm-sized γ' and γ'' precipitates, mostly in the interdendritic regions (Fig. 3). Also revealed by the FEG-SEM is the formation of δ phase particles with their characteristic plate-shaped morphology among the

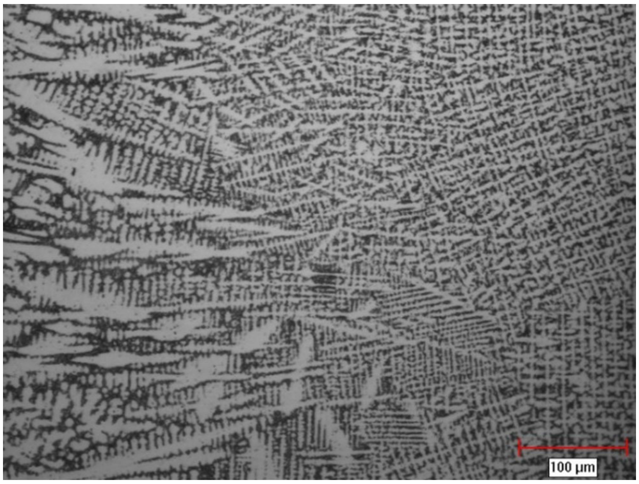

Fig. 1 Optical micrograph showing dendritic microstructure of the fusion zone in the as-weld condition

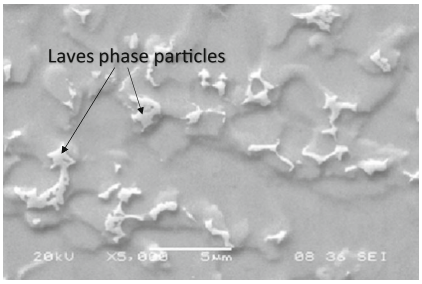

Fig. 2 SEM micrograph showing discontinuous Laves phase particles in the interdendritic region of the fusion zone

interdendritic microconstituents. Transmission electron microscopy study was subsequently performed to unambiguously confirm the nature of the irregular-shaped interdendritic particles and the presence of γ' and γ'' precipitates. TEM X-ray energy-dispersive spectroscopy and selected area diffraction pattern (SADP) analysis show that the interdendritic irregular-shaped particles consist of Laves phase with a hexagonal close-packed crystallographic structure and lattice parameters $a = 0.48$ nm and $c = 0.78$ nm (Fig. 4 and Table 2) and MC-type carbides with a face-centered cubic crystallographic structure and lattice parameter $a = 0.45$ nm (Fig. 5 and Table 2). Analysis of [100] SADP obtained from various regions within the weld fusion zone confirmed the formation of γ' and γ'' precipitates mainly in the interdendritic region (Fig. 6). The formation of the two types of precipitates reduced with increasing distance from the interdendritic regions to the dendrite core regions. Inside the dendrites, only γ' precipitates were formed in the regions close to the interdendritic regions without the γ'' precipitates (Fig. 7), while no evidence of either γ' or γ'' precipitates were observed within the dendrite core regions (Fig. 8)

The distribution of elements in the weld fusion zone of the alloy ATI 718Plus® measured by the partition coefficient k is given in Table 1. The elemental distribution/partition coefficient k, which is defined as the ratio of the concentration of the solute in the solid to that in the liquid in equilibrium to it, was calculated from SEM/EDS data obtained from the dendrite core region near the fusion zone boundary, where the solidification begins. According to Flemings and coworkers [10], under equilibrium conditions, negligible undercooling at the dendrite tips and assuming complete mixing in the liquid and no diffusion in the solid, the solute redistribution can be described by the following equation:

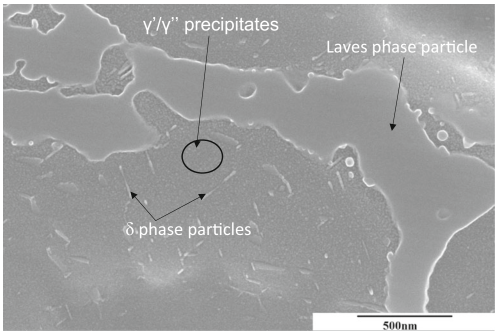

Fig. 3 FEG-SEM showing what appear to be γ'/γ'' precipitates and δ-phase particles in the interdendritic regions of the as-weld fusion zone TIG welded alloy ATI 718Plus®

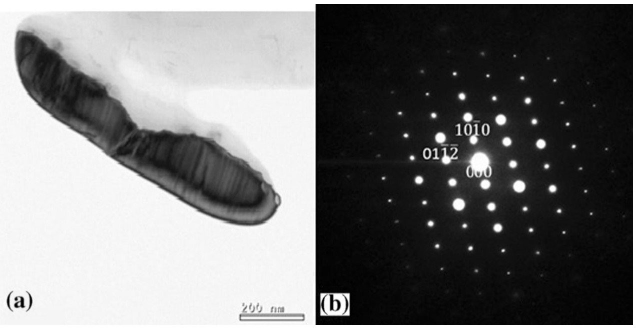

Fig. 4 **a** TEM bright field image showing laves phase, **b** SAD pattern from Laves phase in [022 $\bar{1}$] zone axis

$$C_s = kC_0[1 - f_s]^{(k-1)} \tag{1}$$

Where C_s is the composition of the solid at the liquid/solid interface, C_0 is the nominal composition, and f_s is the volume fraction of the solid. At the start of the solidification, $f_s = 0$, and the first solid to form the liquid (dendrite core), will have a composition of kC_0. Therefore, the ratio between core dendrite composition and the nominal composition of Alloy ATI 718Plus® will yield the partitioning coefficient k at the beginning of solidification.

From Table 1, it is seen that the partition coefficient of Nb and Ti has a value significantly less than 1; this implies that these elements were heavily segregated into the interdendritic liquid during solidification. Similar to the pattern of Nb and Ti, Mo segregated into the interdendritic liquid but in far lesser amount as it has a partition coefficient close to unity. Selective partitioning of Nb, Ti, and C into the interdendritic regions is known to be responsible for the formation of Laves phase particles and MC-type carbides during solidification of the

Table 2 Composition of laves and MC type carbides as obtain from TEM/EDS analysis

Element	Laves		MC	
	Weight%	Atomic%	Weight%	Atomic%
Ti K	1.0	1.4	12.0	18.3
Cr K	14.3	17.6	5.0	7.1
Fe K	6.2	7.1	1.9	2.4
Co K	9.6	10.4	1.2	1.4
Ni K	41.1	44.7	7.4	9.2
Nb K	23.9	16.4	68.9	54.1
Mo K	3.8	2.5	2.9	2.2

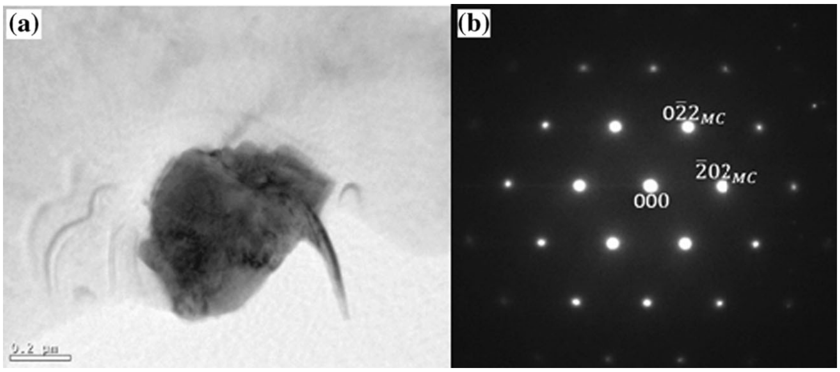

Fig. 5 **a** TEM bright field image showing MC carbide, **b** SAD pattern from MC carbide in [111] zone axis

ATI 718Plus® and Alloy 718 superalloys [6, 9], which is consistent with what is observed in the present work. The other elements in the alloy with k values higher than unity selectively partitioned into the dendrite core. Comparing the partition coefficient k calculated in this work with those reported in previous study on the fusion zone of EBW ATI 718Plus® [6], it is observed that the elemental segregation in both welds follow a similar pattern. However, there is a significant increase in the segregation of Nb and Ti into the interdendritic liquid during the TIG weld solidification as shown by the lower partition coefficient values, which may be due to lower cooling rate enhanced by microsegregation during the cooling of the TIG weld [11]. Moreover, this work shows that the γ'' precipitates, which is rarely reportedly observed in ATI 718Plus®, in the literature, can indeed form due to elemental microsegregation coupled with lower cooling rate during welding. Also, although the γ' precipitates are observed in the as-welded condition, as stated earlier, they do not form uniformly within the weld fusion zone and as such, there is a need for PWHTs to produce uniform precipitation of the strengthening phase. The precipitation behavior of γ' precipitates within the weld fusion zone during PWHT is discussed next.

3.2 Postweld heat treatments

The SEM micrographs in Fig. 9a, b show microstructure of the fusion zone solution heat treated at 982 and 1050 °C, respectively. Partial dissolution of Laves phase particles is observed at 954 and 982 °C solution heat treatments with more dissolution of the Laves particle occurring at 982 °C. It is also observed that δ-phase particles are formed around bulky Laves particles in the interdendritic regions after the solution heat treatments. At 1050 °C solution heat treatment temperature, a complete dissolution of the Laves particles without the formation of the δ-phase particles occurred, as shown in Fig. 9b. The 1050 °C heat treatment temperature is reported to be above the solvus temperature of δ-phase particles [1].

After the aging heat treatment of solution heat-treated specimens, γ' phase is observed to have precipitates all through the fusion zone as can be seen in the SEM micrographs shown in Fig. 10. No γ'' precipitates are observed in the aged treated sample. It is possible that the γ'' precipitates formed after welding dissolved during the PWHT. The precipitation kinetics of γ' precipitates in the fusion zone and base material in the temperature range of 650 to 950 °C for 1 min–1 h are represented on the time-temperature-transformation (TTT) curve

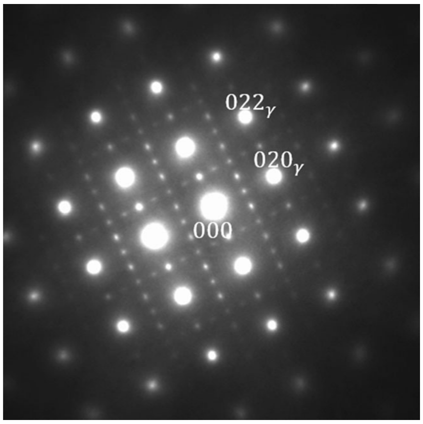

Fig. 6 TEM analysis: Selected area diffraction pattern in [100] matrix zone axis showing diffraction spots from γ'' precipitates. SAD is taken from an area close to Laves phase

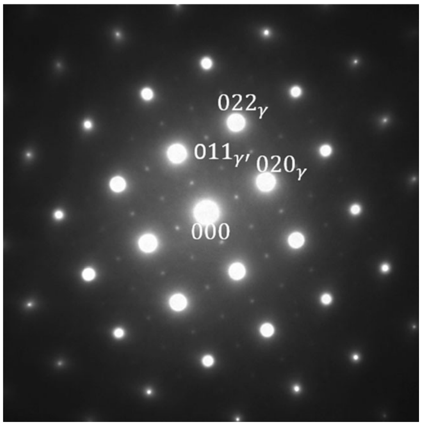

Fig. 7 Selected area diffraction pattern in [100] matrix zone axis showing diffraction spots from γ' precipitates only. SAD is taken from an area away from Laves phase

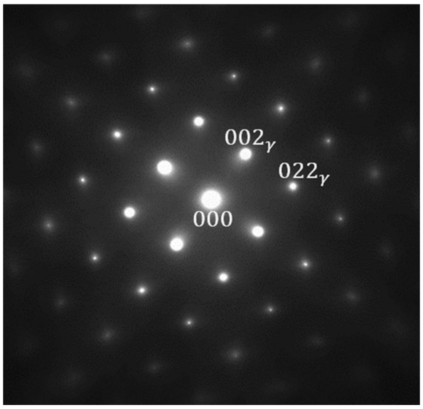

Fig. 8 Selected area diffraction pattern from [100] matrix zone axis. Note the very weak super lattice diffraction spots in SADP suggesting that γ' precipitates have formed but these might be very small

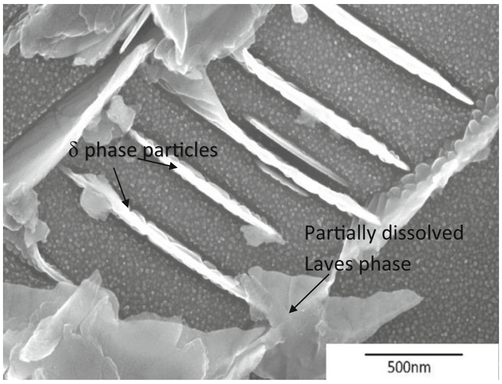

Fig. 10 A high magnification FEG-SEM micrograph of the fusion zone after recommended heat treatment showing partially dissolved Laves phase particles and newly formed delta phase in addition to a high volume fraction of γ' precipitates

shown in Fig. 11a. The specimens were first solution heat-treated at 1000 °C/1 h and water quenched to completely dissolve γ' and γ'' precipitates that had formed in the specimens during welding. The Vickers microhardness after this treatment was 265 and 235 HV for the fusion zone and the base material, respectively. The precipitation of γ' is taken to have started when the hardness value exceeds 265 and 235 HV. It can be seen from the TTT curve that the rate of precipitation of γ' phase is much slower in the fusion zone compared to the base material at higher temperatures. This difference in the precipitation kinetic between the base material and the fusion zone however becomes insignificant below

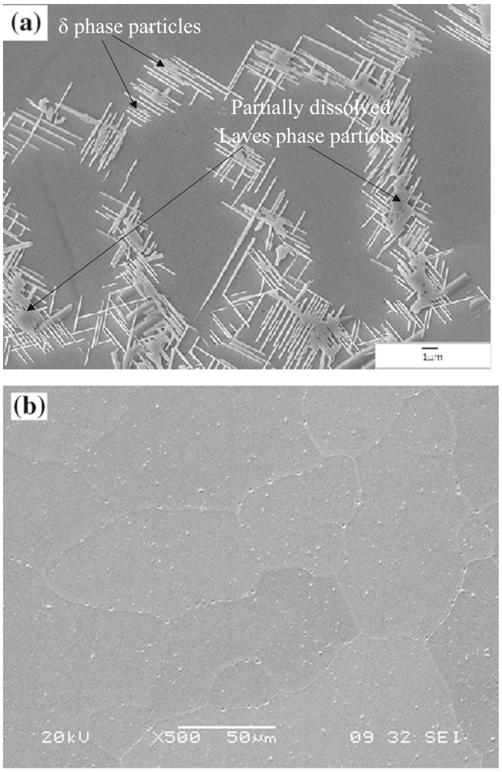

Fig. 9 SEM micrographs of the fusion zone **a** at 954 °C solution treatment temperature showing partial dissolution of Laves phase and precipitation of δ phase **b** at 1050 °C solution treatment temperature showing complete dissolution of Laves phase with no precipitation of δ phase

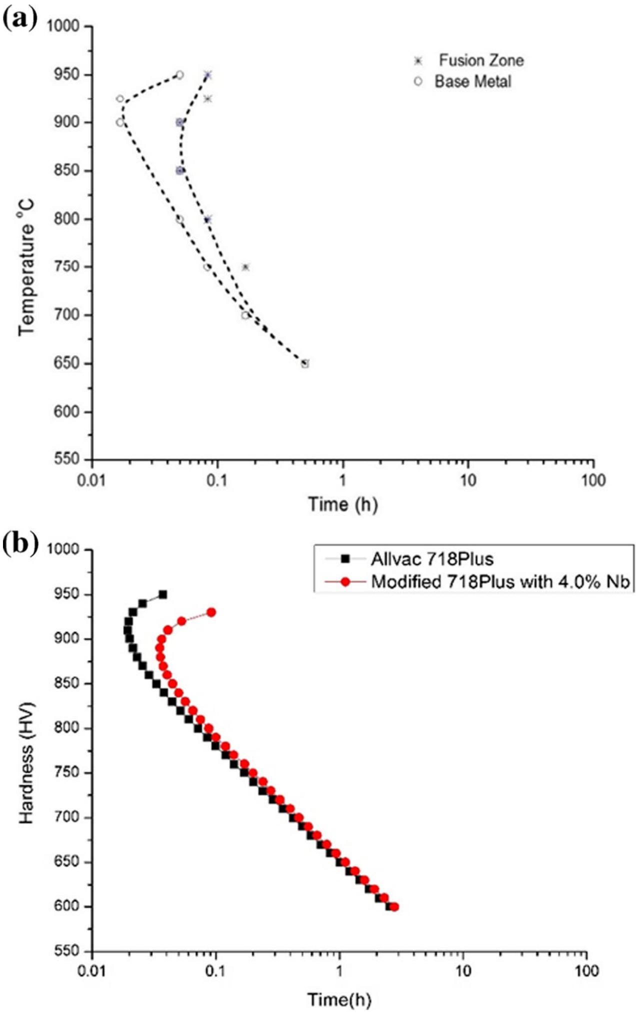

Fig. 11 **a** A TTT curves of γ' precipitation in the fusion and base metal of ATI 718Plus® measured by hardness. **b** A TTT-curve of γ' ATI 718Plus® and modified ATI 718Plus® (with less Nb) calculated by JMatPro

750 °C. A clear picture of the difference in precipitation kinetics of γ' can be seen in Fig. 12. The slower observed response to aging treatment of the fusion zone compared to the base material may be related to the depletion of the Nb and Ti elements from the fusion zone dendrite core regions as a result of microsegregation that occurred during weld solidification. Complete dissolution of Laves phase particles and redistribution of the segregated Nb in the fusion zone during solution heat treatment is rather difficult to achieve because of the poor diffusivity of the large Nb atoms [12, 13]. Therefore, the core fusion zone dendrite is still expected to be significantly deficient in Nb compared to the interdendritic region after solution heat treatment. A TTT curve of γ' phase calculated by JMatPro of a typical ATI 718Plus® and also of a modified alloy ATI 718Plus® in which the Nb content was reduced (4 %Nb) is shown on Fig. 11b. It is seen in the calculated Java-based Materials Properties (JMatPro) TTT curves that Nb content in the alloy ATI 718Plus® can affect the precipitation kinetics of the alloy and that lower Nb content reduces the rate of precipitation during the aging treatment.

The peak hardness values of the fusion zone for all the solution heat-treated specimens at 954, 982, and 1050 °C are observed to be comparable after aging at different temperatures, which is also observed to be similar to the peak hardness value of the base material in the recommended heat-treated condition as presented on Fig. 13 . It can, thus, be deduced that notwithstanding the depletion of Nb from the gamma matrix to form Laves phase particles in the interdendritic regions after standard PWHT, as seen in Fig. 10a, sufficient γ' precipitates formation still occurred to adequately strengthen the alloy to the level of the base material that is free of the Laves phase. This is in contrast to the case of Alloy 718 fusion zone [9] where the depletion of Nb to form interdendritic Laves phase particles is reported to affect

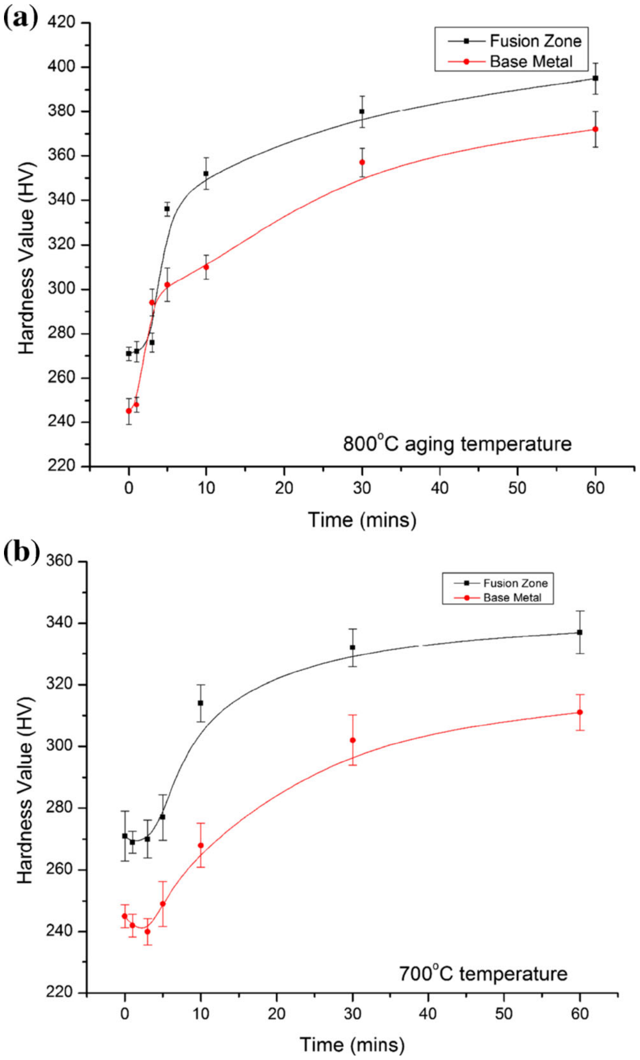

Fig. 12 Isothermal aging curves of ATI 718Plus® comparing the precipitation kinetics of fusion zone and the base metal at **a** 800 and **b** 700 °C

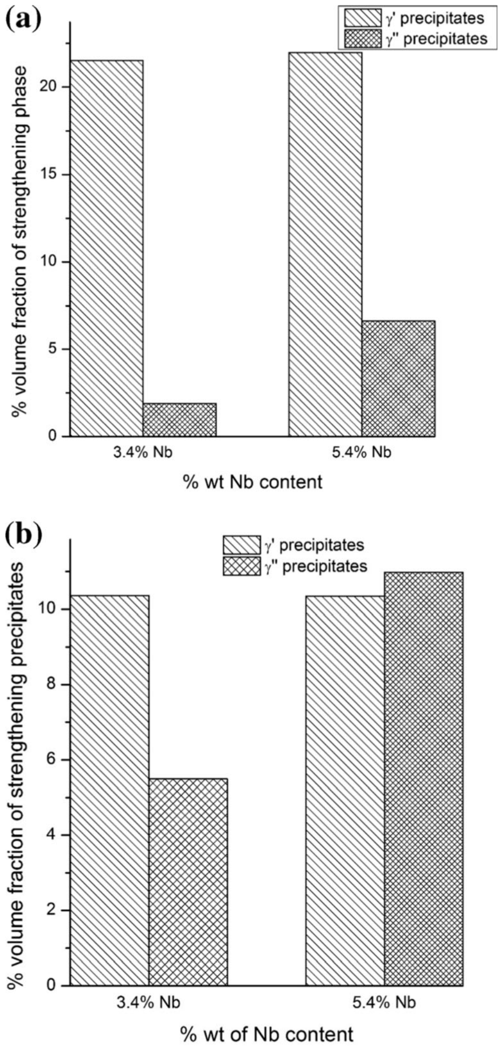

Fig. 13 JMatPro modeling showing the effect of Nb content on the volume fraction of the strengthening phase **a** ATI 718Plus® and **b** Alloy 718

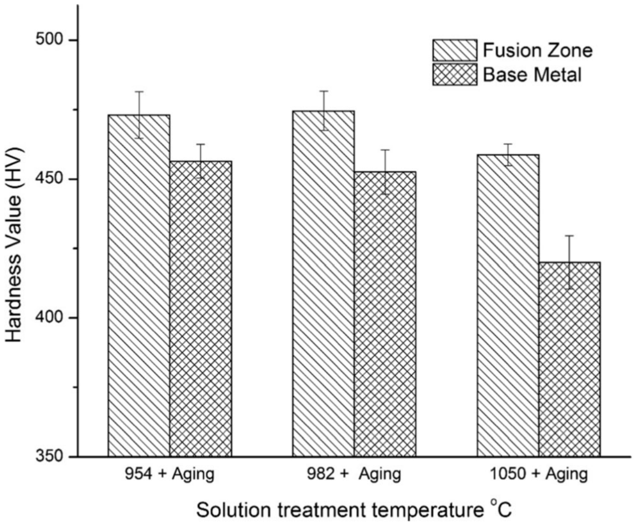

Fig. 14 Hardness value as a function of solution treatment temperature in the fusion zone of aged alloy ATI 718Plus®

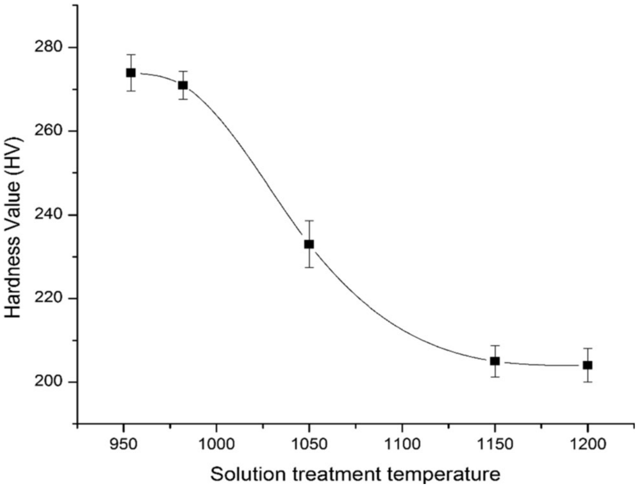

Fig. 15 Hardness value as function of solution treatment temperature

the extent of precipitation of the strengthening phase in the alloy, γ'' precipitates. The γ'' phase in Alloy 718 requires considerable amount of Nb for its formation [13] and so the depletion of Nb from the dendrite core affects the extent of its formation during PWHTs. However, the γ' phase in ATI 718Plus® requires much less Nb for its formation and so the depletion of Nb from the dendrite core does not affect the formation of γ' phase precipitates in the required volume fraction to adequately strengthen the alloy ATI 718Plus®. This could explain the difference in the effect of Nb microsegregation on the extent of precipitation of the strengthening precipitates in the two alloys. The influence of Nb concentration on the volume fraction of γ' and γ'' in Alloy 718 and ATI 718Plus® is calculated using the JMatPro presented on Fig. 14. It is seen that the effect of Nb content is drastic in Alloy 718 as the volume faction of the main strengthened phase γ'' is significantly reduced from 11 to 5.5 % vol. when the Nb concentration in the alloy is reduced from 5.4 to 3.4 % wt Nb. However, in ATI 718Plus®, the volume faction of the main strengthening phase γ' remain almost the same when the Nb concentration in the alloy is reduced from 5.4 to about 3.4 % wt Nb. The simulated results using JMatPro and the hardness values from experiments agree and indicate that Nb segregation from the dendrite core during welding have minimal effect on the volume fraction of γ' precipitates in ATI 718Plus® but could have significant effect on the volume fraction of γ'' precipitates in Alloy 718 alloy.

The influence of solution heat treatment temperature, used prior to aging, on hardness value of the fusion zone is presented in Fig. 15. The hardness value of the fusion zone starts to significantly decrease as the solution heat treatment temperature rises above 982 °C. This observation can be explained by the dissolution of Laves phase particles at these temperatures, without the formation δ phase particles that have pinning effect on grain boundary migration [14, 15]. As shown in Fig. 9b, there seems to be complete dissolution of the Laves particles in the fusion zone with no evidence of δ-phase particles at 1050 °C solution heat treatment temperature and above. An increase in grain size due to this heat treatment may be responsible for the decrease in the hardness observed. Likewise, there is a significant loss of hardness in the base material solution heat treated at 1050 °C solution temperature prior to aging (Fig. 13) which may also be related to the rapid grain growth that occurred at the 1050 °C due to the dissolution of δ-phase particles.

The influence of cooling rate from the solution heat treatment temperature on the hardness value aging treatment is presented in Fig. 16. It is observed that there is no significant difference in the hardness values of the specimens cooled at 25 °C/s (air-cooled) and 500 °C/s (water-quenched), but there is considerable decrease in the hardness value for the specimen cooled at 0.25 °C/s (furnace-cooled). Furnace cooling (0.25 °C/s) appears to have aided the nucleation and growth of the γ' precipitates in the fusion zone during cooling from

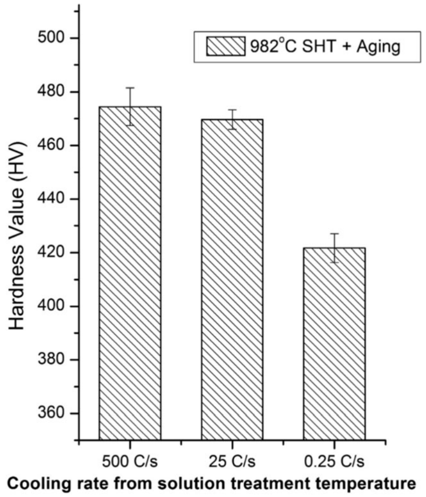

Fig. 16 Hardness as a function of cooling rate in the fusion zone of standard aged alloy ATI 718Plus®

solution heat treatment temperature and subsequent aging heat treatment. The average size of the γ' precipitates in the furnace-cooled specimen after aging is about 50–70 nm, which is about two times the size of the γ' precipitates in the aged specimens that were air-cooled and water-quenched. The precipitation strengthening in this alloy is achieved by two main strengthening mechanisms—the shearing and non-shearing mechanisms [16–18]. The operative strengthening mechanism in the alloy, under a given condition, depends on the size of the γ' precipitates [16]. To achieve optimum strength, the γ' precipitate size in the alloy should be such that the precipitates are coherent with the γ matrix and also have a strong and shearable interaction with an approaching dislocation [16]. The peak size that confines the regime of coherent and shearable precipitates is reported to be around 20–30 nm [16, 19]. Continuous aging beyond this peak size may cause the γ' precipitates to lose its coherency or no longer capable of being sheared by dislocation, and at this point, the non-shearable strengthening mechanism commences. In the present work, the precipitate size in furnace-cooled samples suggests that perhaps non-shearing mechanism is operative, which does not have as much strengthening effect as the shearing mechanism, thereby causing reduction in the observed hardness compared to air-cooled and water-quenched conditions.

3.3 Summary and conclusions

The main findings of this study can be summarized as follows:

1. TIG welding results in increased elemental microsegregation, compared to EBW, in ATI 718Plus® alloy, with Nb and Ti segregating extensively into the interdendritic liquid during weld solidification.
2. The elemental microsegregation in the TIG welds of the alloy ATI 718Plus® resulted in the formation of Laves phase particles, MC-type carbides, and delta-phase particles in the interdendritic regions.
3. Furthermore, in contrast to what has been reported in EBW of the ATI 718Plus® alloy, non-homogenous precipitation of γ' and γ'' occurred in the TIG welds, due to enhanced microsegregation and lower cooling rate caused by the higher heat input involved during the TIG welding.
4. Theoretical calculations and experimental observation showed that notwithstanding Nb being a γ' phase forming element, it is the precipitation kinetics and not the extent of γ' precipitate formation during PWHTs that is reduced by the microsegregation of Nb that occurred during the weld solidification.

Acknowledgments The authors gratefully acknowledge financial support from the NSERC of Canada. The help of Dr. A. Khan with the TEM work is gratefully acknowledged

References

1. Cao W-D (2005) Solidification and solid state phase transformation of ALLVAC® 718plus™ alloy: in superalloys 718, 625, 706 and derivatives 2005. In: Loria EA (ed) TMS (The Minerals, Metals & Materials Society). North Carolina, USA, pp 166–177
2. Kennedy WD, Cao RL (2005) New development in wrought in 718-type. Acta Metall 18(1):39–46
3. Kennedy WD, Cao RL (2004) Role of chemistry in 718-type alloy-Allvac 718Plus alloy development: in superalloys. In: Pollock TM, Harada H, Green KA (eds) TMS (The Minerals, Metals & Materials Society). North Carolina, USA, pp 91–99
4. Xishan X, Jianxin D, Gailian W, Wei Y (2005) The effect of Nb, Ti, Al on precipitation and strengthening behavior of 718 type superalloys: in superalloys 718, 625, 706 and derivatives 2005. In: Loria EA (ed) TMS (The Minerals, Metals & Materials Society). North Carolina, USA, pp 289–298
5. Bayha TD, Lu M, Kloske KE (2005) Investment casting of ALLVAC® 718Plus™ alloy: in superalloys 718, 625, 706 and derivatives, 2005. TMS (The Minerals, Metals & Materials Society). North Carolina, USA, pp 223–232
6. Vishwakarma KR, Richards NL, Chaturvedi MC (2008) Microstructural analysis of fusion and heat affected zones in electron beam welded ALLVAC® 718PLUSTM superalloy. Mater Sci Eng A 480:517–528
7. Andersson J, Sjo¨berg GP (2012) Repair welding of wrought superalloys Alloy 718, Allvac 718Plus and Waspaloy: Institute of Materials, Minerals and Mining. Science and Technology of Welding and Joining 17(1):49–59
8. Idowu OA, Ojo OA, Chaturved MC (2009) Crack-free electron beam welding of Allvac 718Plus superalloy. Weld J 88:179–187
9. Janaki Ram GD, Venugopal Reddy A, Prasad Rao K, Madhusudhan G (2005) Microstructure and mechanical properties of Inconel 718 electron beam welds: Institute of Materials, Minerals and Mining. Mater Sci Technol 21:1132–1138
10. Bower TF, Brody HD, Flemings MC (1966) Measurements of solute redistribution in dendritic solidification. AIME Met SocTrans 236:624–634
11. Fredriksson T, Antonsson H (2005) The effect of cooling rate on the solidification of INCONEL 718. Metallurg Mater Trans B 36B:85–96
12. Cao X, Rivaux B, Jahazi M, Cuddy J, Birur A (2009) Effect of pre- and post-weld heat treatment on Metallurgical and tensile properties of Inconel 718 alloy butt joints welded using 4 kW Nd:YAG laser. J Mater Sci 44:4557–4571
13. Radavich JF (1989) The physical metallurgy of cast and wrought alloy 718: in superalloy 718. In: Loria EA (ed) The Minerals, Metals & Materials Society, pp 229–240
14. Pickering EJ, Mathur H, Bhowmik A, Messe OMDM, Barnard JS, Hardy MC, Krakow R, Loehnert K, Stone HJ, Rae CMF (2012) Grain-boundary precipitation in Allvac 718Plus. Acta Mater 60: 2757–2769
15. Song K, Aindow M (2008) Grain growth and particle pinning in a model Ni-based superalloy. Mater Sci Eng A 479:365–372
16. Ahmadi MR, Povoden-Karadeniz E, Whitmore L, Stockinger M, Falahati A (2014) Yield strength prediction in Ni-base alloy

718Plus based on thermo-kinetic precipitation simulation. Mater Sci Eng A 608:114–122

17. Whitmore L, Ahmadi MR, Stockinger M, Povoden-Karadeniz E, Kozeschnik E, Leitnera H (2014) Microstructural investigation of thermally aged nickel-based superalloy 718Plus. Mater Sci Eng A 594:253–25
18. Whitmore L, Ahmadi MR, Guetaz L, Leitner H, Povoden-Karadeniz E, Stockinger M, Kozeschnik E (2014) The microstructureofheat-treatednickel-basedsuperalloy718Plus. Mater Sci Eng A 610:39–45
19. Whitmore L, Leitner H, Povoden-Karadeniz E, Radis R (2012) Transmission electron microscopy of single and double aged 718Plus superalloy. Mater Sci Eng A 534:413–423